PERGAMON

International Journal of Heat and Mass Transfer 42 (1999) 3481–3494

International Journal of HEAT and MASS TRANSFER

Conditional analysis of turbulent heat transport in a quasi two-dimensional wake interacting with a boundary layer

G.A. Sideridis, E.G. Kastrinakis, S.G. Nychas*

Department of Chemical Engineering, Aristotle University of Thessaloniki, University Box 453, 54006 Thessaloniki, Greece

Received 29 July 1998; received in revised form 4 December 1998

Abstract

A conditional averaging technique has been used for the analysis of experimental data obtained from heat flux measurements in the region of interaction of a cylinder wake with a boundary layer. The circular cylinder was placed normal to the flow and parallel to a flat plate, just outside of the boundary layer. The surface of the cylinder was intentionally rough, following our observation that in this way the velocity power spectrum in the intermediate wake could be forced to acquire some quasi two-dimensional turbulence characteristics, namely to display a scaling region deviation from the $-5/3$ power law which is characteristic of homogeneous, three-dimensional turbulence. The streamwise and the normal (to the plate) velocity components, as well as the temperature at the same position, have been recorded simultaneously, using hot wire anemometry. Time variations of the relevant Reynolds shear stress and heat fluxes were evaluated directly from the experimental data. These results were then conditionally averaged according to the quadrant splitting analysis technique. It was found that in the boundary layer region, a particular fluid motion ('ejections', in the quadrant splitting analysis terminology) dominate the flow. That motion is the main carrier of hot fluid from the boundary layer to the wake.

1. Introduction

Complex flows similar to the present one of a turbulent wake interacting with a boundary layer, may be encountered in many engineering applications. The associated entrainment and mixing processes influence directly phenomena like heating and cooling, chemical reaction progress, aerodynamic performance, dispersion of atmospheric pollutants, etc. The primary mechanism of entrainment is large-scale engulfment. This is followed by mixing and diffusion which are related to small-scale perturbations [1,2]. Large-scale coherent structures present in a turbulent wake play an important role in both entrainment and mixing. This is because these structures are associated with large-scale motions and also with small-scale turbulence production due to vortex stretching [3]. Mass transport resulting from such phenomena is difficult to measure directly. For that reason, mass transport may be simulated by heat transport based on the fact that the Prandtl and Schmidt numbers for gases are both close to one. Consequently, the mass and heat diffusivities are of the same order.

The turbulent wake examined in the present work is that of a circular cylinder. The strong coherent structures present in the wake, the von Kaŕmán vortices, have attracted the interest of researchers for many years [4,5]. An extensive description of their topological details and properties has been presented by Hussain and Hayakawa [6]. They reported that the von Kármán vortices retain their well-defined staggered organization, their strong coherent nature, and their periodicity throughout the intermediate wake (10

* Corresponding author.

0017-9310/99/$ - see front matter
PII: S0017-9310(99)00013-7

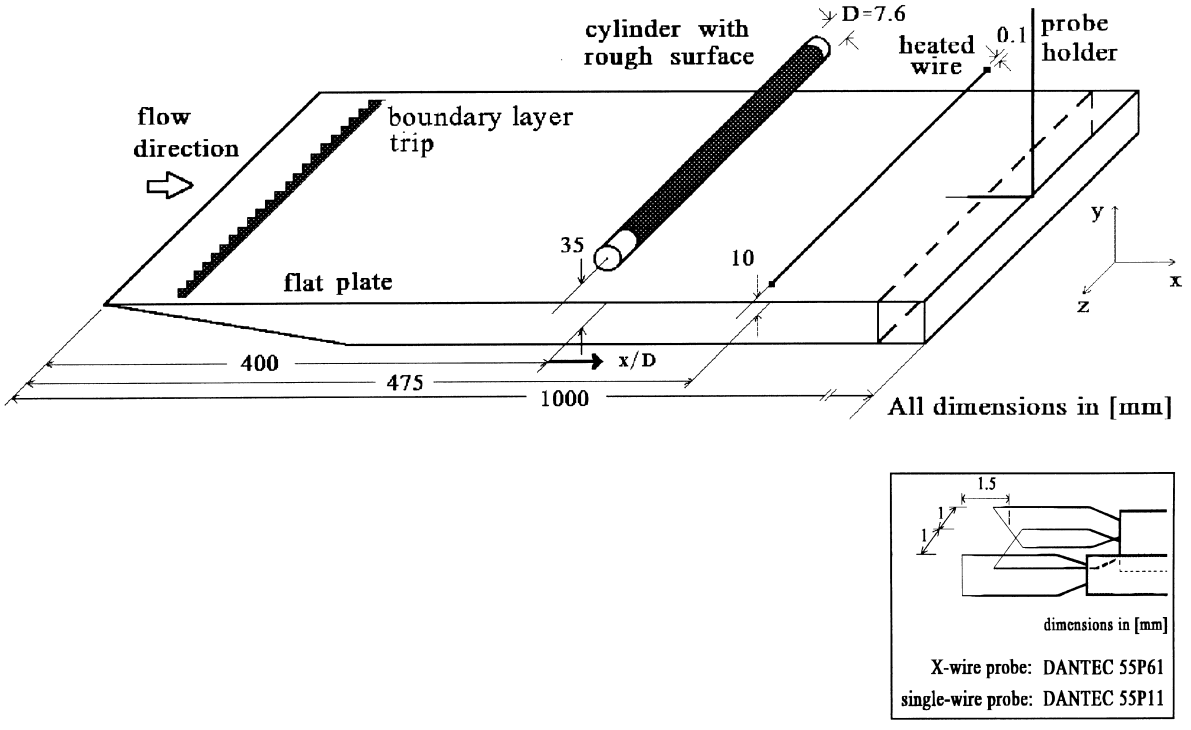

Fig. 1. The experimental set-up and the triple-wire probe used.

$< x/D < 50$, D=cylinder diameter). Further away from the cylinder, the vortices start to break up, producing a flow with different type and degree of organization in the wake [7]. Rather few experimental studies of the case of a cylinder wake interacting with a boundary layer, in either isothermal or non-isothermal conditions, may be found in the literature. Usually, the cylinder is immersed in the boundary layer and vortex formation characteristics are examined [8,9]. In non-isothermal conditions, most experimental research works present temperature and heat flux measurements in the far wake of a slightly heated isolated cylinder [10,11]. Matsumura and Antonia [12] examined the contribution from the coherent motion to the time-averaged momentum and heat fluxes and they provided detailed description of the topology of the velocity and temperature fields. In addition, Wroblewski and Eibeck [13] measured turbulent heat fluxes and Reynolds stresses in a heated boundary layer disturbed by an embedded streamwise vortex.

Numerical simulation of a vortex interacting with a flat plate boundary layer have been considered much more extensively [14]. Usually, a single, two-dimensional vortex is examined, travelling in a free stream and passing close enough to a wall to interact with the boundary layer [15]. It is very difficult to produce such 'pure' flows in the laboratory for validation of numerical methods. Usually, a series of vortices is produced (e.g. a von Kármán street of vortices) which have some two-dimensional characteristics, but essentially, they are three-dimensional. It is generally accepted that quasi two-dimensional turbulence is characterized by the existence in the velocity power spectrum of a scaling region following a power law with exponent deviating from the value $-5/3$, which is typical for isotropic, three-dimensional turbulence. For quasi two-dimensional turbulence, this value is -3 [16]. An example of a real flow with such velocity power spectrum characteristics is the high-altitude atmospheric flow [17].

In order to produce experimental results in the present study that can be used for validation of numerical models and perhaps for a qualitative investigation of the atmospheric flow, particular attention was given to the promotion of the two-dimensional characteristics of the present flow. During an earlier work [18], it was found that a cylinder with a rough surface produced a wake with a velocity power spectrum displaying an exponent $-7/3$ in a region bounded by the limits: $y'/D < \pm 2$, $10 < x/D < 40$ at a Reynolds number R_D within the range: $1500 < R_D < 3000$ (D is the cylinder diameter, y' is measured from the wake centerline). For that reason, the experimental results reported in this

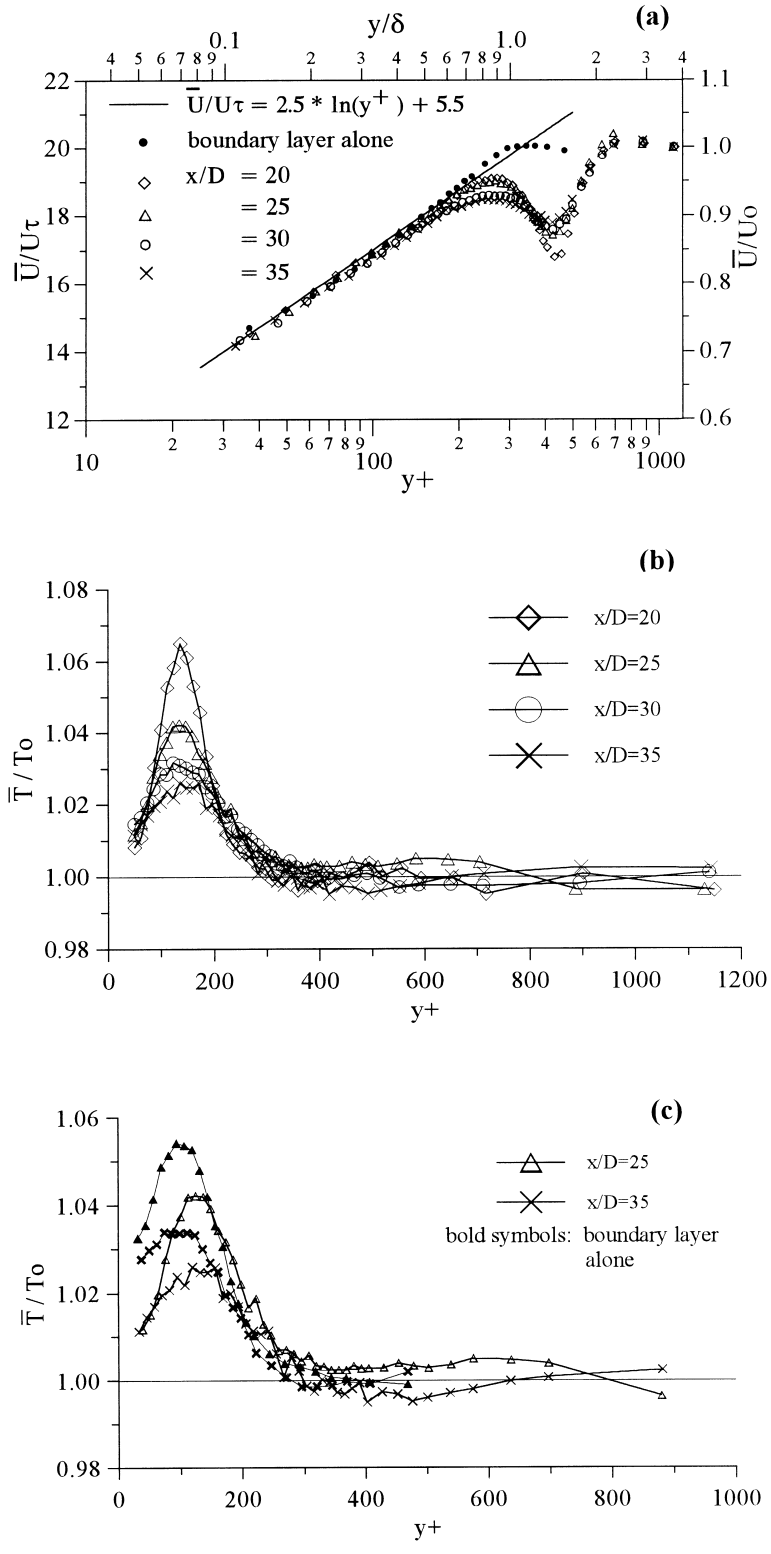

Fig. 2. Mean streamwise velocity and mean temperature profiles for both the wake–boundary layer and the boundary layer alone configurations.

work were produced using a circular cylinder covered with high-grade sand paper.

2. Experimental procedure

The present experimental work was conducted in an open return, suction type wind tunnel. The dimensions of the test section were $0.3 \times 0.3 \times 2$ m and the free stream turbulence level was less than 0.4%. The configuration used is shown in Fig. 1. Special care was devoted to position the plate in the test section with its top surface parallel to the main flow in order to avoid flow separation at the sharp leading edge. Nevertheless, the boundary layer was tripped near the leading edge to ensure fully turbulent flow development along the plate. A tripping device like the one proposed by Hama [19] was used. It consisted of a row of thin triangular patches pasted on the surface of the plate. A spiral motion is promoted in the space between two neighboring triangles, resulting in consistent three-dimensional vortex shedding, which tripped the boundary layer.

The diameter of the cylinder used was $D=7.6$ mm and it was located at a height above the plate, $h_c=5D$. The local boundary layer thickness was $\delta_o \sim 3D$. (δ_o is defined as the length normal to the surface within which the local mean velocity $\bar{U}_{(y)}$ varies from 0 to 99% of the free-stream velocity.) Hence, $(h_c/\delta_o) \sim 1.6$. The value of h_c was such that the von Kármán vortices were formed within the free stream, well above the boundary layer, but close enough for interaction to occur at a streamwise distance of about $10D$. Heat was supplied to the boundary layer flow by means of an electrically heated wire with diameter 0.1 mm, as it is shown in Fig. 1. It was producing a peak temperature rise in the flow of about 1.5°C. The flat plate was an isothermal surface.

Hot-wire anemometry was used throughout the present measurements. The triple-wire probe, shown in Fig. 1, was used. It consisted of an X-wire probe for the measurement of the instantaneous values of two velocity components and a single (cold) wire probe, for the simultaneous recording of temperature. The cold wire was placed 1 mm apart and 1.5 mm ahead of the double hot wire probe, in order to avoid thermal interaction. The probe was operated by a multi-channel anemometer system, type AN-1003 of A.A. Laboratory Systems Ltd. The probe output signals were digitized by an 8-channel 16-bit analog to digital converter (type Data Translation DT-2809) and then they were fed to a personal computer for processing. Sampling frequency was 4 kHz per channel and 163,000 samples were acquired per channel.

The triple wire probe was calibrated as follows (a detailed description of the technique may be found in a publication by Papanikolaou et al. [20]): The probe was placed in a jet of air that could be heated electrically. Keeping the jet velocity constant, the electric power supplied to the heating device was increased in steps. As soon as the jet reached a steady state after each increment, the cold wire output voltage was recorded and plotted against the jet temperature provided by a thermocouple. Four such data points were sufficient to determine the cold wire calibration curve (a straight line). For the calibration of the hot wire X-probe, the jet was heated gradually, at constant mass flow rate. This was performed by applying a suitable electric power over 10 min to raise the jet temperature by about 60°C above the ambient. During this period, the cold and hot wire outputs were recorded simultaneously. The jet temperature was evaluated using the cold wire calibration curve. From that, the jet velocity was determined, using the perfect gas law. The procedure is repeated at several jet mass flow rates, thus providing a hot-wire calibration databank.

During the present experiments, the triple-wire probe recorded simultaneously the streamwise and the normal velocity components $U(t)=\bar{U}+u(t)$, $V(t)=\bar{V}+v(t)$ and temperature $T(t)=\bar{T}+T'(t)$ (an overbar denotes time-averaged values and lower-case letters or a prime, denote fluctuations). The estimated maximum error in the measurement of the velocity and temperature fluctuation terms is 2.5 and 1%, respectively. Time variations of the two heat flux components $uT'(t)$, $vT'(t)$ and the momentum flux $uv(t)$ were evaluated by digital post-processing. Throughout the present experiments, the free stream velocity was $U_o=3.5$ m/s, giving $R_D=1820$. The friction velocity U_τ, referred to the plate and obtained from a $(U_o-U_{(y)})/U_\tau$ vs y/δ_o Clauser plot, was $U_\tau=0.175$ m/s. The probe was traversed from a point well within the free stream, to a distance of 4 mm from the surface of the plate, at the four measuring stations in the streamwise direction: $x/D=20$, 25, 30 and 35.

3. Results

3.1. Mean flow

Profiles of the normalized mean velocity $\bar{U}/U_o$ and temperature $\bar{T}/T_o$ (T_o = ambient temperature) plotted against normalized distance from the plate y^+ ($=U_\tau y/\nu$, where U_τ is the friction velocity and $\nu=0.146\times10^{-6}$ m^2/s, the kinematic viscosity of air), are shown in Fig. 2. Included with the mean velocity profiles for the present experimental configuration (Fig. 2a), there is a profile measured at the same experimental conditions but with the cylinder removed from the set-up. A single profile of the mean velocity distribution from the isolated boundary layer case is shown, because it

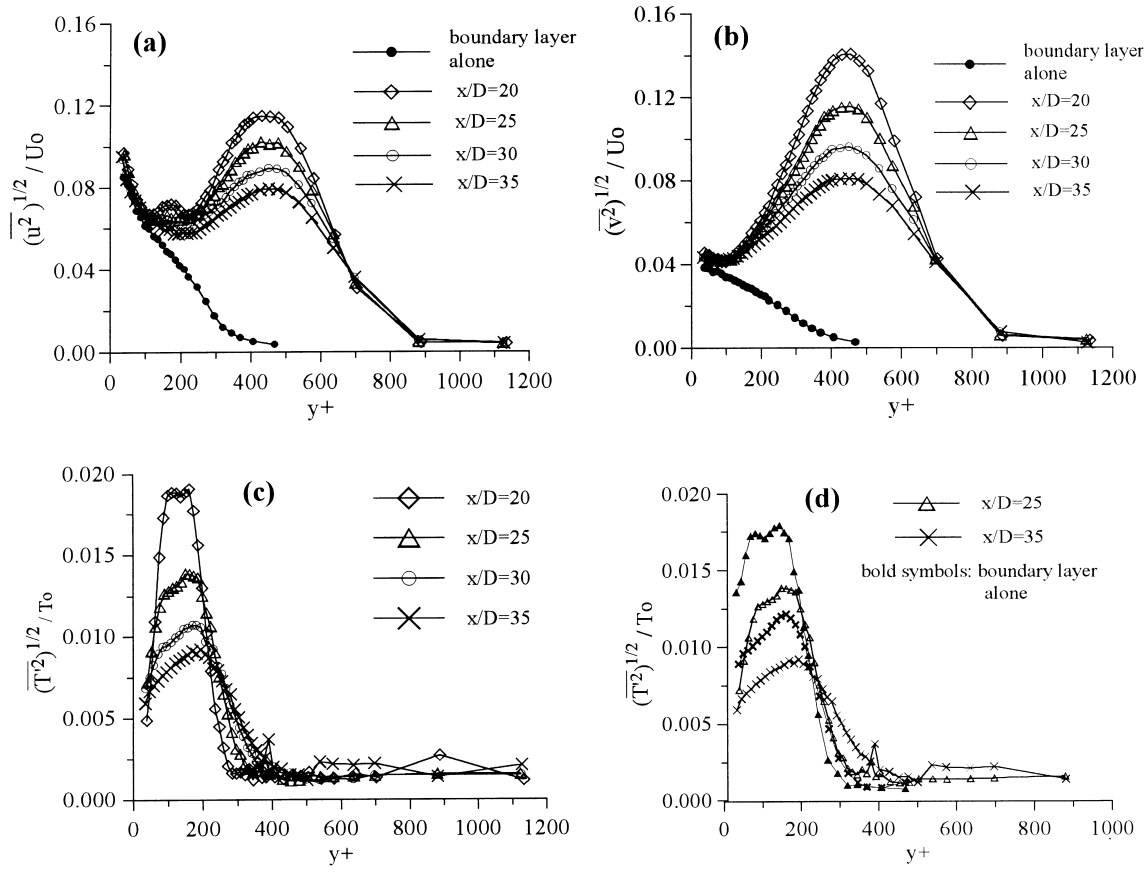

Fig. 3. Profiles of the r.m.s. values of two velocity components and temperature for both the wake–boundary layer and the boundary layer alone configurations. In (a) and (b) the boundary layer data shown were measured at $x/D=20$ but they are identical at any other station.

was found that all profiles at the aforementioned x/D locations collapse onto each other. A logarithmic scale has been used in the velocity profiles plot for comparison with a logarithmic law, typical of fully turbulent flow. As indicated in Fig. 2(a), the lower part of the velocity profiles ($30 < y^+ < 200$) coincide with the logarithmic law, denoting a fully turbulent boundary layer flow without significant effects from the cylinder. The upper part of the profiles ($200 < y^+ < 800$, in the complete configuration) display a velocity defect, as expected within the wake of the cylinder. The maximum velocity defect is defined at every streamwise location as follows: $U_d = U_o - U_{min}$ (U_{min} = minimum velocity in the wake). The mean temperature excess T_e behind the heated wire remains appreciable at all measuring stations (Fig. 2b). Here, $T_e = T_{max} - T_o$, where T_{max} is the maximum temperature behind the heated wire. Representative mean temperature data for the boundary layer alone case and the corresponding profiles for the complete configuration are compared in Fig. 2c. It is evident that the complete configuration profiles have lower peaks which are shifted towards higher y^+-values. Also, these profiles expand towards higher y^+-values more than the isolated boundary layer profiles. These results give a clear indication of the important role of the cylinder wake in heat transport away from the plate.

Fig. 3 presents r.m.s. velocity and temperature fluctuation profiles for both configurations considered. Peak values of both velocity fluctuation components in the cylinder wake region decrease with distance downstream as a result of the continuous weakening of the von Kármán vortices. The irregularities in the profiles near $y^+ = 170$ are due to thermal cross-talk in the wake of the heated wire. Close to the plate ($y^+ < 100$) all complete configuration profiles coincide with the representative boundary layer alone profile, indicating in this way the extent of the effect of the wake onto the boundary layer. The r.m.s. temperature profiles for the wake–boundary layer configuration (Fig. 3c), show clearly the progressive spreading of heat normal to the plate, presumably as a result of the wake

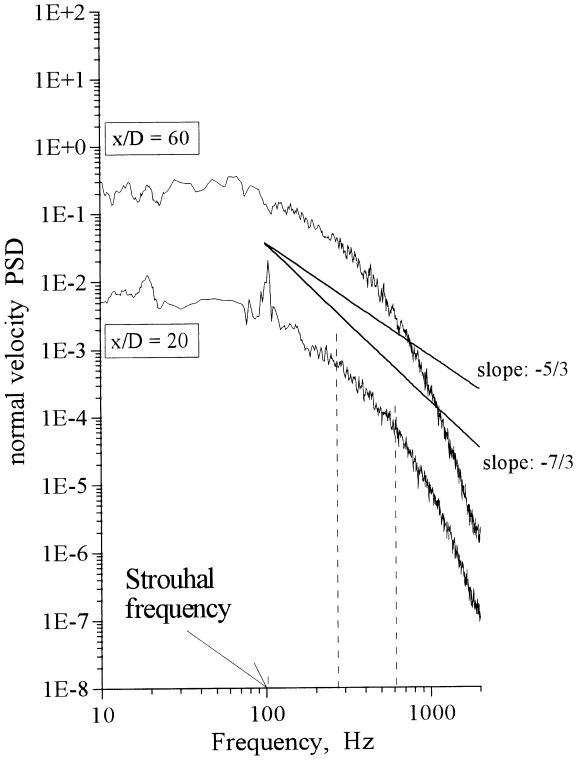

Fig. 4. Typical normal velocity power spectra at $x/D=20$, 60.

interaction. This argument is supported by the data appearing in Fig. 2d, where corresponding r.m.s. temperature fluctuation profiles are compared.

3.2. Velocity power spectra

Fig. 4 displays typical normal velocity power spectra for the present flow. Both curves shown were obtained at $y^+=260$. They were found to be the same throughout the width of the wake at the corresponding streamwise locations. At $x/D=20$, a well-defined peak at the Strouhal frequency (98 Hz) indicates the presence of strong von Kármán vortices. Also, it can be seen that a scaling region exists with slope $-7/3$, extending from about 250 to 600 Hz (marked by broken lines), implying a quasi two-dimensional flow. It has been observed that these characteristics become weaker as the streamwise distance from the cylinder increases. That occurs much earlier in the lower half-wake than in the upper, presumably due to the interaction with the boundary layer. It may be noted here that the aforementioned characteristics are still distinguishable in the upper half wake at $x/D=40$.

There is no evidence in the normal velocity power spectrum distribution at $x/D=60$ of the existence of von Kármán vortices in the flow. Furthermore, there is no part in the scaling region with slope close to $-7/3$. At the lower frequencies, the scaling region has slope equal to $-5/3$. At the higher frequencies, the slope attains values much higher than $-7/3$.

3.3. Conventionally time-average momentum and heat fluxes

Conventional time-averages of momentum and heat fluxes $\overline{uv}(y^+)$, $\overline{uT'}(y^+)$, $\overline{vT'}(y^+)$, normalized by U_d and T_e (in order to locate self-similar evolutions within the wake), are presented in Fig. 5. $\overline{uv}(y^+)$ displays two peaks, one at each half-wake, with considerable difference in their absolute values. The smaller peak, in the lower half-wake, is the direct result of the interaction with the boundary layer. It may also be observed that all curves except that for $x/D=35$, coincide with each other, indicating self-similarity of the flow, almost up to $x/D=30$. Close to the plate, the distinct troughs near $y^+=170$ at $x/D=20$, 25 are attributed to thermal cross-talk in the wake of the heated wire. Streamwise heat flux appears to be confined to the undisturbed boundary layer thickness (of about 300 y^+-units, Fig. 5b). On the contrary, normal heat flux expands continuously along the y^+-direction (Fig. 5c).

The effect of the wake on $\overline{uv}$, $\overline{uT'}$ and $\overline{vT'}$ may be seen in the plots presented in Fig. 6. Here, U_o and T_o have been used for normalization since the boundary layer flow region is of interest. Fig. 6a shows that the wake influences the boundary layer flow much closer to the plate than the mean and r.m.s. velocity data have indicated (Figs. 2a and 3a,b). Fig. 6b and c shows clearly that the presence of the wake has very little effect on $\overline{uT'}$ and a very drastic effect on $\overline{vT'}$, thus confirming the conclusion mentioned earlier that $\overline{uT'}$ is confined to the undisturbed boundary layer thickness and that $\overline{vT'}$ expands rapidly above the undisturbed boundary layer thickness.

In order to examine these observations in greater detail and also the associated mechanisms of scalar transport, a conditional analysis technique was applied, described in the following section.

3.4. Quadrant splitting analysis

This method is based on splitting the instantaneous $uv(t)$ signal into four sectors (or 'quadrants'). Each one is associated with one of the four possible combinations of the instantaneous values of $u(t)$ and $v(t)$ in terms of their signs [21], i.e.:

$u>0$, $v>0$:	1st	quadrant	(outward interactions)
$u>0$, $v>0$:	2nd	$-/-$	(ejections)
$u>0$, $v>0$:	3rd	$-/-$	(wallward interactions)
$u>0$, $v>0$:	4th	$-/-$	(sweeps)

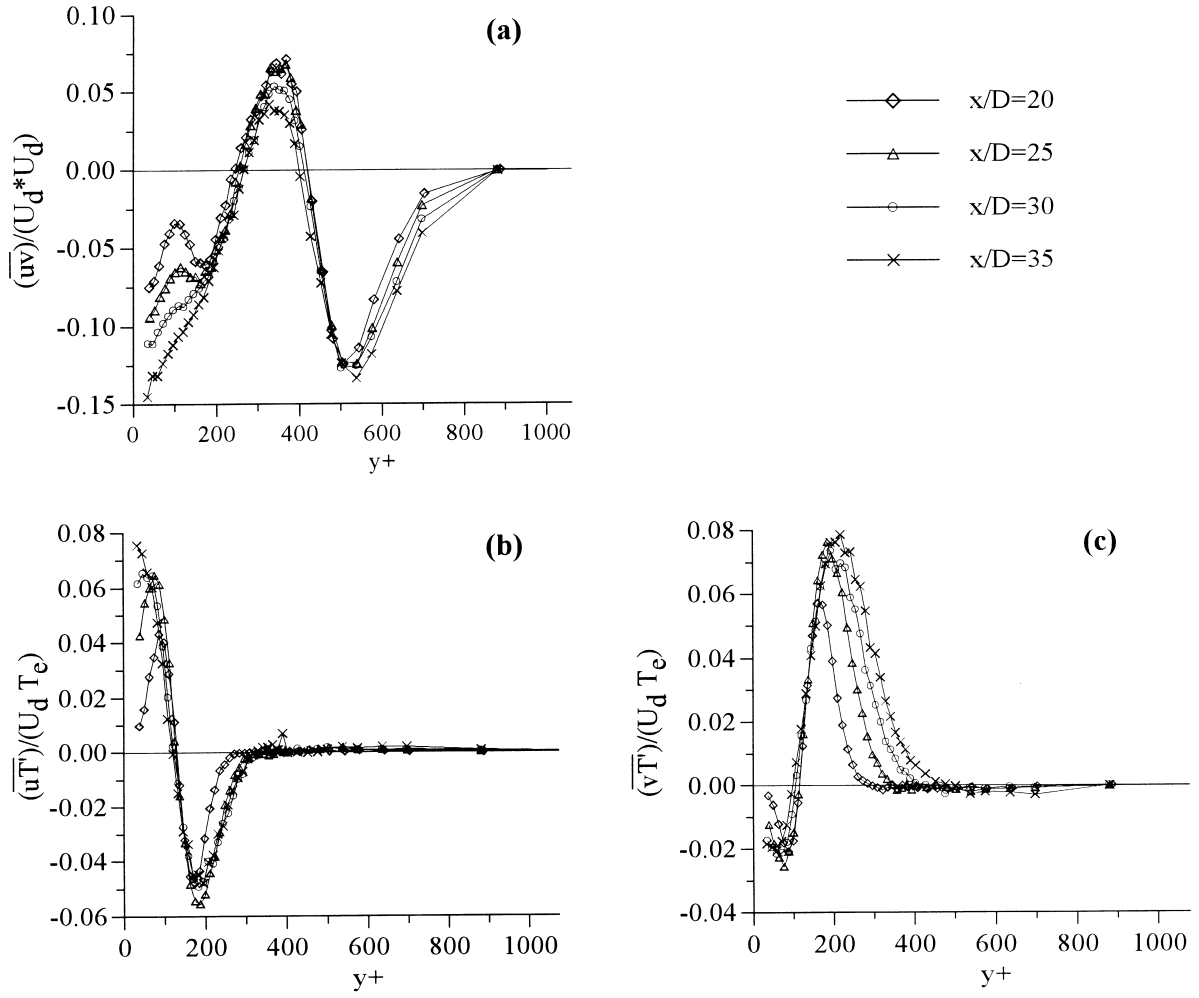

Fig. 5. Distributions of conventionally time-averaged momentum and heat fluxes.

(The names of the four quadrants correspond to visually observed wall structures in fully developed pipe and channel flows.) The time-average of $uv(t)$ in each quadrant is finally calculated, thus providing at each measuring point four conditionally averaged values for the momentum flux.

We have extended the application of this method by treating each of the $uT'(t)$ and $vT'(t)$ signals in the same way as $uv(t)$. Hence, the magnitudes of $\overline{uT'}$ and $\overline{vT'}$ at every measuring point were in effect analyzed into contributions from each of the four elementary fluid motions. Angular brackets $\langle\rangle$ in Figs. 7–10 have been used to denote this conditional averaging.

During a preliminary investigation, the effect of using some threshold for each of the $u(t)$ and $v(t)$ signals was examined. Two threshold values have been tested: 1 and 0.1 times the r.m.s. values of $u(t)$ and $v(t)$. Representative results are shown in Fig. 7, where the distribution normal to the plate of the conditionally averaged momentum flux is presented. The shape of the curves does not appear to be affected appreciably by the threshold value. Furthermore, certain characteristics of the curves shown, e.g. peaks, are more clearly discriminated at the higher threshold value. Hence, the latter has been retained for the remaining calculations. Because of that thresholding, it may be argued that the quadrant splitting analysis results in the wake are related primarily to the periodic motion, whereas in the boundary layer region, they refer to the strong coherent motions.

3.4.1. Conditionally averaged momentum flux

Distributions of conditionally averaged momentum flux are shown in Fig. 8 for various streamwise positions. It is noted here that the magnitude of $\langle\overline{uv}\rangle$ at

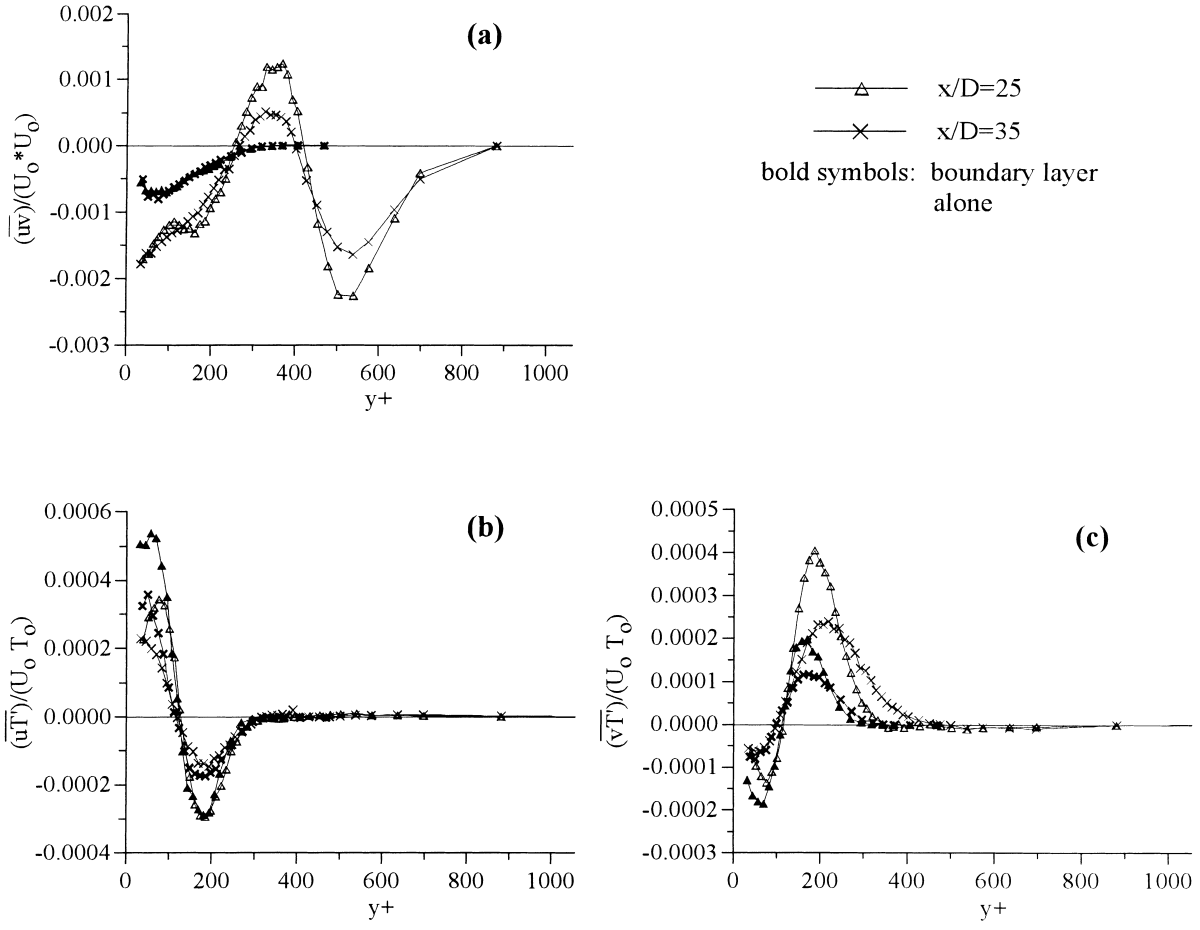

Fig. 6. The effect of the wake on the momentum and heat fluxes distributions.

each y^+-location is indicative of the relative strength of the four elementary fluid motions. Hence, as it can be seen in Fig. 8, the strongest motions within the boundary layer are ejections and sweeps. The magnitude of sweeps is nearly constant with both y^+ and x/D, whereas the magnitude of ejections increases very rapidly approaching the wall and as the streamwise distance x/D increases. It must be emphasized, however, the fact that the streamwise development of ejections has been exaggerated due to the normalization method chosen (the velocity defect U_d decreases with x/D). If the elementary flows in the wake region are referred to the wake center line (the line $y^+ = 440$), they can be distinguished into two types: those pointing towards it and those pointing away from it, either in an upstream or downstream direction relative to the mean flow. Fig. 8 shows that in that sense, ejections may be related to wallward interactions and sweeps, to outward interactions. The combined distribution of each pair is symmetric about the wake center line. There is no appreciable development in the streamwise direction of either the distribution or the magnitude of the elementary flows. Most affected are sweeps and outward interactions which have been subjected to an overall reduction of their magnitudes. Hence, it may be concluded that in each half-wake, the strongest motion is in the outward (relative to the wake centerline) and upstream (relative to the mean flow) directions.

3.4.2. Conditionally averaged heat fluxes

The conditionally averaged heat flux components in the streamwise and normal directions are presented in Figs. 9 and 10, respectively. Each plot shows the contribution of each of the elementary motions. Furthermore, by looking at the sign of the heat flux components at any y^+-location, and the sign of the associated velocity component, it can be deduced whether that heat flux is related to the transport of hot or cold fluid (in the present work, cold refers to a tem-

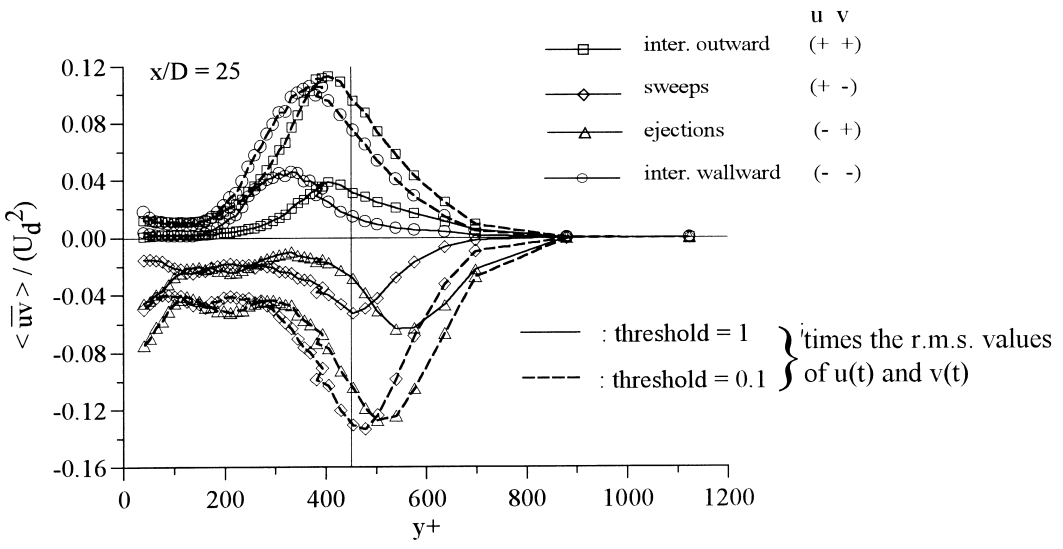

Fig. 7. The effect of the threshold value on the conditionally averaged momentum flux.

perature lower than the mean temperature). It is evident from Figs. 9 and 10 that the events with primary contributions to heat flux are ejections and sweeps. At $y^+ > 150$, i.e. above the thermal wake of the heated wire, ejections are associated with hot fluid and sweeps with cold. The contribution from the wallward interactions, which are associated with cold fluid transport, although negligible at $x/D = 20$, it becomes progressively more appreciable further downstream. Its significance lies in the fact that it has opposite sign to that of the streamwise heat flux contributions of sweeps and ejections, causing the overall time-averaged $\overline{uT'}$ to appear confined to the boundary layer flow (refer to Section 3.3 and Fig. 5). The contribution of the outward interactions, associated with hot fluid transport, is present only at $x/D = 30$, 35 and at $y^+ > 200$. Below the thermal wake of the heated wire, i.e. at $y^+ < 150$, the only contribution to the streamwise and normal heat fluxes are from ejections and sweeps. It can easily be deduced from the examination of the signs of the parameters involved that these motions have exchanged their roles: ejections carry cold fluid and sweeps, hot.

It is also evident from the plots in Figs. 8 and 9 that the distribution of $\langle\overline{uT'}\rangle$ and $\langle\overline{vT'}\rangle$ due to ejections and sweeps, except of a moderate overall reduction of their magnitudes with x/D, they retain their original features in the streamwise direction. This fact, attributed to the normalization method chosen, denotes that there is no drastic evolution of hot and cold fluid transport in the streamwise direction by ejections and sweeps. Furthermore, it may also be concluded that there is no direct dependence to the wake–boundary layer interaction process. On the other hand, there is a well-defined streamwise evolution of the heat flux contributions due to the wallward and outward interactions. That, together with the fact that this evolution takes place in the vicinity of the wake–boundary layer interaction region, leads to the conclusion that this heat flux is a direct result of activities emanating from that region.

3.4.3. Heat flux vector plot

Considering the sections of the conditionally averaged heat flux distribution which are related to hot fluid transport only (denoted by subscript h) and regarding $\langle\overline{uT'}\rangle_h$ and $\langle\overline{vT'}\rangle_h$ at every point in the present flow as the magnitudes of the heat flux vectors along the horizontal and vertical directions respectively, hot fluid transport is presented in Fig. 11 in vector form, according to the relation:

$$\vec{Q}_h = [\langle\overline{uT'}\rangle_h / U_d T_e]\mathbf{i} + [\langle\overline{vT'}\rangle_h / U_d T_e]\mathbf{j} \quad (1)$$

where $\mathbf{i}$ and $\mathbf{j}$ are unit vectors along the streamwise x/D-and normal y^+-directions, respectively. $\vec{Q}_h$ is thus the heat flux vector in the $x/D-y^+$ plane, depicting hot fluid transport only, according to the information presented in Figs. 9 and 10. It is noted here that in the calculation of $\langle\overline{uT'}\rangle_h$ and $\langle\overline{vT'}\rangle_h$, the velocity fluctuation components $u(t)$ and $v(t)$ have been used. Consequently, $\vec{Q}_h$ is referred to the local mean velocity and therefore, it may appear in Fig. 11 pointing in the upstream direction.

The following sequence of events may be deduced from the Fig. 11: ejections originating near the plate (i.e. at very small y^+ values), initially carry cold fluid through the hot region created by the heated wire

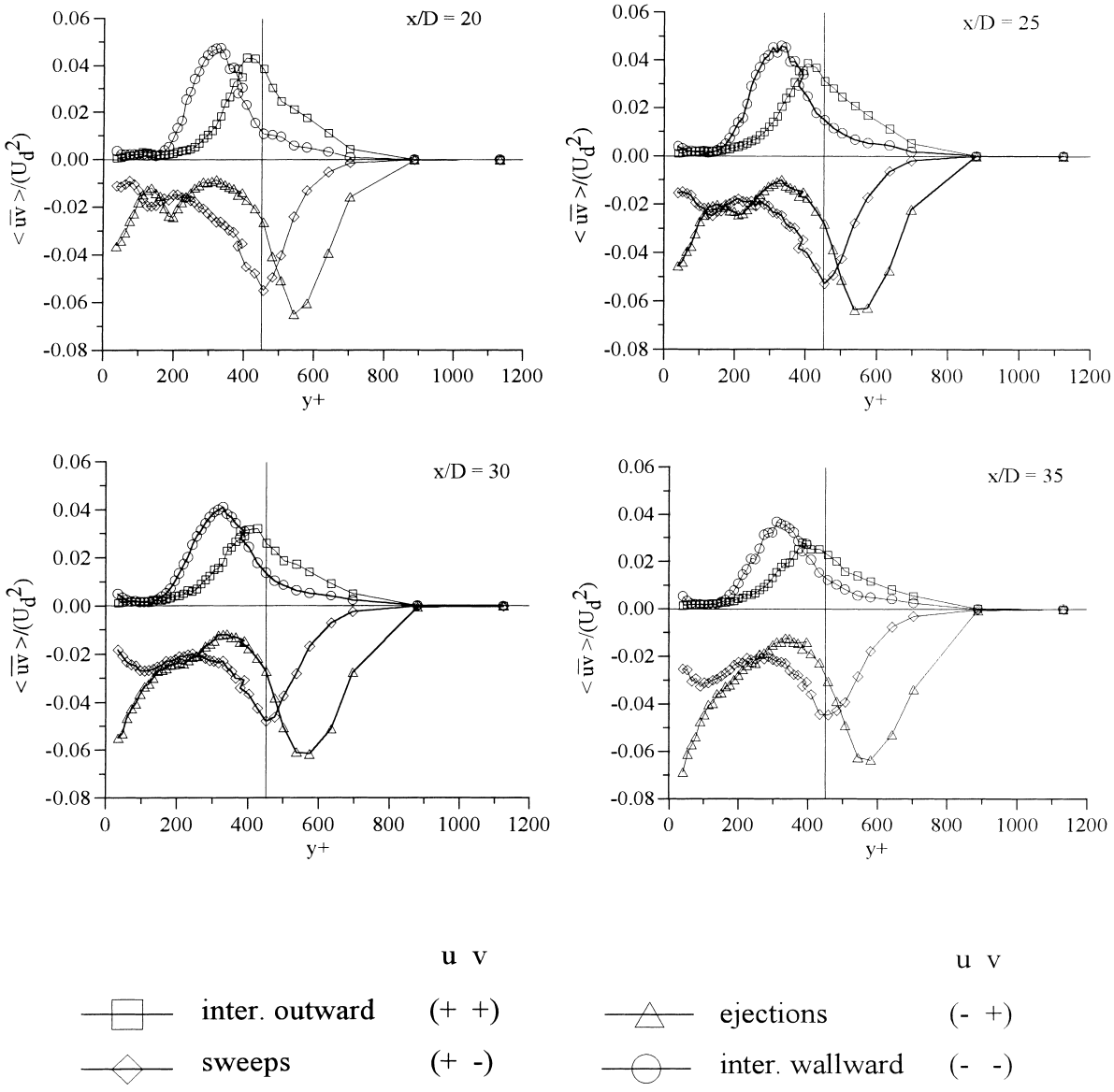

Fig. 8. Distributions of the conditionally averaged momentum flux. The cylinder is located at $y^+ = 440$.

(marked in Fig. 11 by the dotted lines). This newly heated fluid is then carried away, again by ejections, towards higher y^+ values (motion A in Fig. 11). At $x/D = 30$, 35 and at $200 < y^+ < 350$ another hot fluid motion appears (motion C), which is attributed to large-scale activities in the wake. In a similar manner, sweeps coming from large y^+ values, well within the wake, move cold fluid through the hot region and then, they carry the hot fluid just produced towards the plate (motion B).

An independent phase-averaging analysis indicates that fluid motions carrying heat away from the wall region are related to flow structures induced by the passage of the von Kármán vortices [22].

4. Conclusion

The present experimental results suggest that in the flow under investigation, two basic processes have major contributions to the heat flux observed. These flows are ejections and sweeps, in the quadrant splitting analysis terminology. Ejections carry hot fluid from the boundary layer region to the wake and

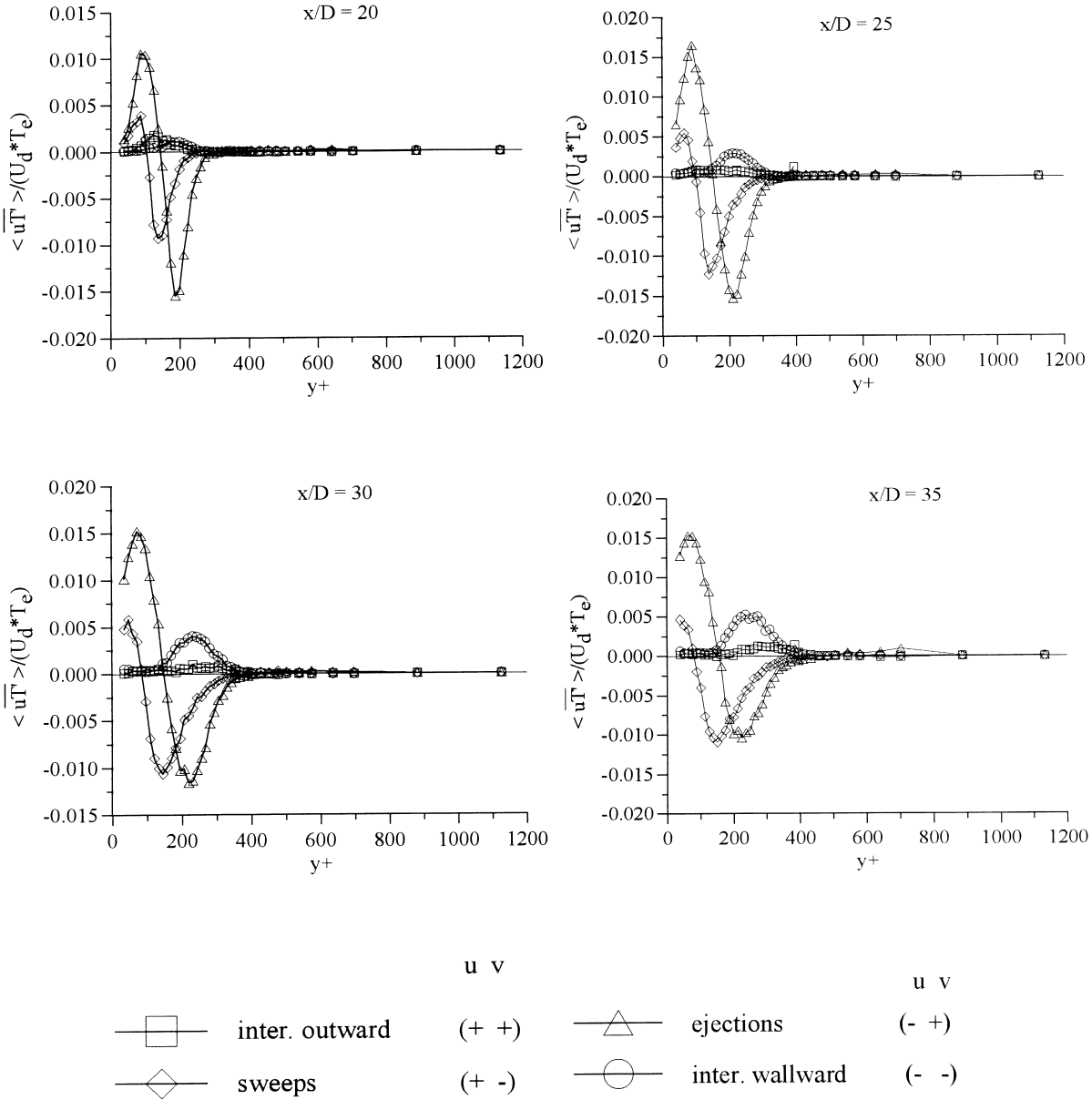

Fig. 9. Distributions of the four basic flows contributions to the streamwise heat flux.

sweeps transport cold fluid from the wake towards the boundary layer. These activities appear to be part of a continuous process, without significant evolution in the streamwise direction, except for a well-defined spreading in the normal direction to the plate. Minor heat flux contributions, however, due to the flows classified as outward and wallward interactions, are related to processes that evolve in the wake–boundary layer interaction region and hence, they can be regarded as direct results of that interaction.

Acknowledgement

The present work was supported by the European Communities Commission under contract No. AVI-CT92-0017.

References

[1] J.J. Turner, Turbulent entrainment: the development of

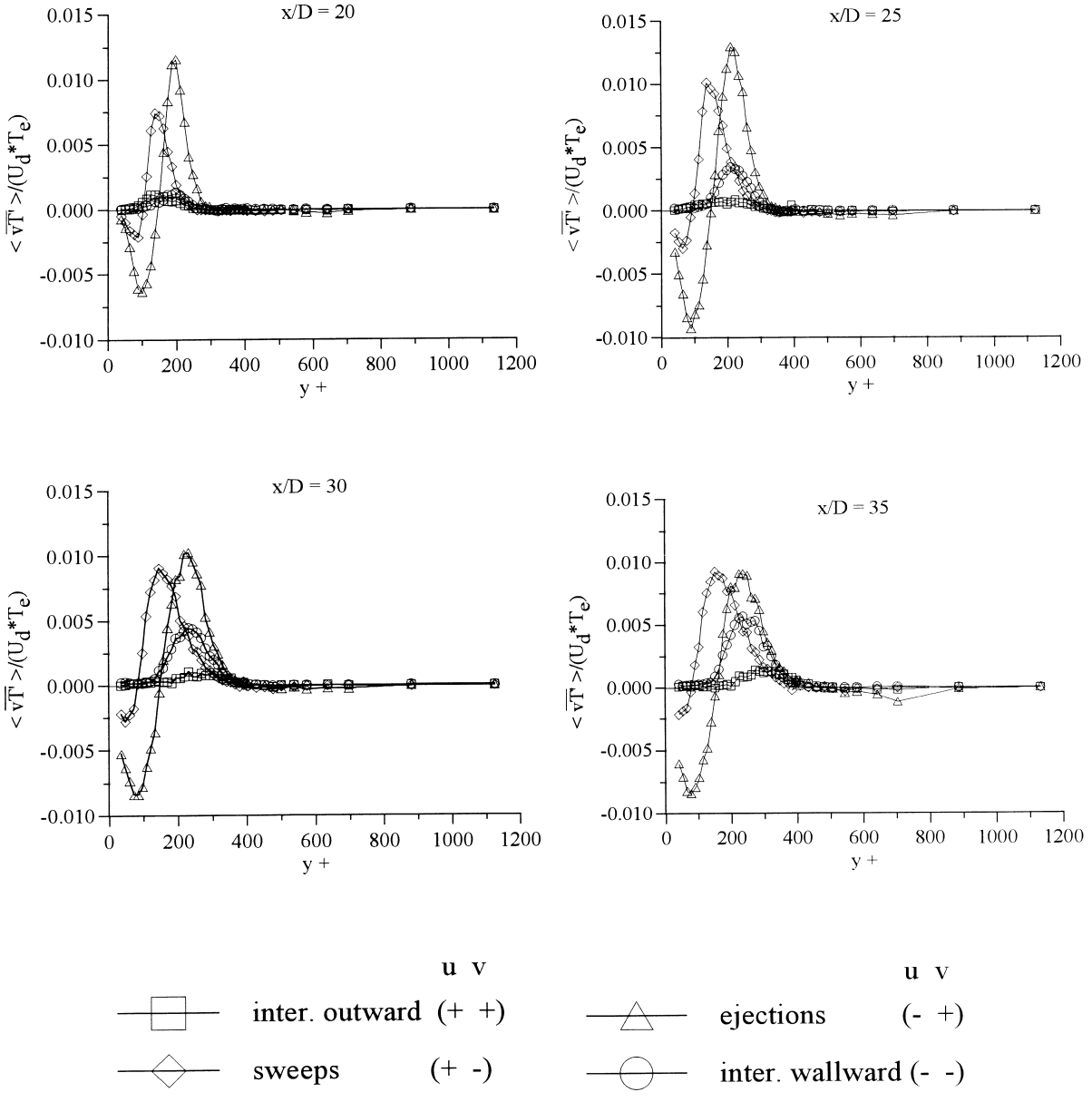

Fig. 10. Distributions of the four basic flows contributions to the normal heat flux.

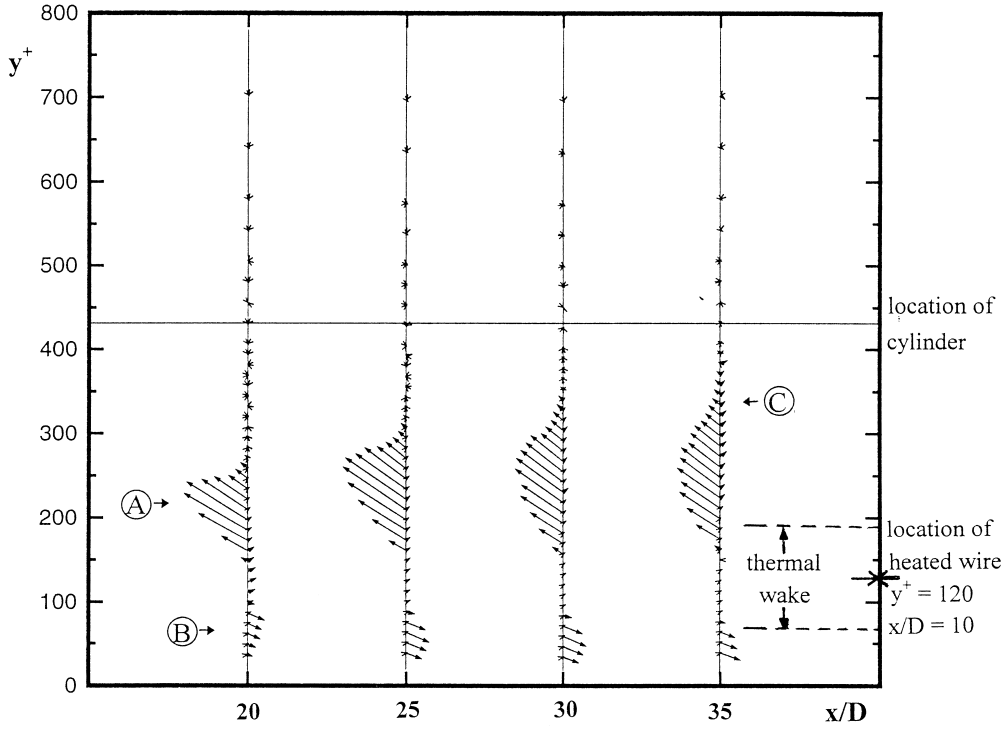

Fig. 11. Vector plot of heat flux (only due to hot fluid transport). The flow direction is left to right. The frame of reference moves with the mean velocity. Ⓐ, Ⓑ: primary heat flux due to fluid motions with u: −, v: + ('ejections') and u: +, v: − ('sweeps'), respectively. Ⓒ: secondary heat flux due to fluid motions with u: +, v: + ('outward interactions'). The flow with u: −, v: − ('wallward interactions'), does not carry hot fluid.

the entrainment assumption and its application to geophysical flows, J. Fluid Mech. 173 (1986) 431–471.
[2] S.J. Lin, G.M. Corcos, The mixing layer: deterministic models of a turbulent flow, Part 3. The effect of plane strain on the dynamics of streamwise vortices, J. Fluid Mech. 141 (1984) 139–178.
[3] A.K.M.F. Hussain, Coherent structures and turbulence, J. Fluid Mech. 173 (1986) 303–356.
[4] D.J. Tritton, Physical Fluid Dynamics, 2nd ed., Oxford Science, 1988.
[5] M. Kiya, M. Matsumura, Turbulence structure in the intermediate wake of a circular cylinder, Bull. JSME 28 (1985) 2617–2624.
[6] A.K.M.F. Hussain, M. Hayakawa, Eduction of large-scale organized structures in a turbulent plane wake, J. Fluid Mech. 180 (1987) 193–229.
[7] J.A. Ferrè, J.C. Mumford, A.M. Savill, F. Giralt, Three-dimensional large-eddy motions and fine-scale activity in a plane turbulent wake, J. Fluid Mech. 210 (1990) 371–414.
[8] D.W. Bearman, M.M. Zdravkovich, Flow around a circular cylinder near a plane boundary, J. Fluid Mech. 89 (1978) 33–47.
[9] K. Suzuki, H. Suzuki, V. Kikkawa, H. Kigawa, Study on a turbulent boundary layer disturbed by a cylinder—effect of cylinder size and position, in: Proceedings of the Seventh Symposium on Turbulent Shear Flows, Stanford University, 1989, pp. 8.5.1–8.5.6.
[10] G. Fabris, Conditional sampling study of the turbulent wake of a cylinder. Part I, J. Fluid Mech. 94 (4) (1979) 673–709.
[11] J.A. Ferre, F. Giralt, Some topological features of the entrainment process in a heated turbulent wake, J. Fluid Mech. 198 (1989) 65–78.
[12] M. Matsumura, R.A. Antonia, Momentum and heat transport in the turbulent intermediate wake of a circular cylinder, J. Fluid Mech. 250 (1993) 651–668.
[13] D.E. Wroblewski, P.A. Eibeck, Measurements of turbulent heat transport in a boundary layer with an embedded streamwise vortex, Int. J. Heat Mass Transfer 34 (7) (1991) 1617–1631.
[14] T.L. Doligalski, C.R. Smith, D.A. Walker, Vortex interactions with walls, Annu. Rev. Fluid Mech. 26 (1994) 573–616.
[15] A. Luton, S. Ragab, D. Telionis, Interaction of spanwise vortices with a boundary layer, Phys. Fluids 7 (11) (1995) 2757–2765.
[16] H. Tennekes, Turbulent flow in two and three dimensions, Bull. Amer. Meteor. Soc. 59 (1978) 22–28.
[17] G.J. Boer, T.G. Sepherd, Large-scale, two-dimensional turbulence in the atmosphere, J. Atmos. Sci 40 (1983) 165–184.

[18] G.A. Sideridis, E.G. Kastrinakis, S.G. Nychas, Experimental simulation of air pollution dispersion by atmospheric motions, in: H. Power, N. Moussiopoulos, C.A. Brebbia (Eds.), Proceedings of the Air Pollution III Conference, Vol. 2, Computational Mechanics Publications, Boston, Southampton, 1995, pp. 177–184.

[19] F.R. Hama, An efficient tripping device, J. Aero. Sci. 24 (1957) 236–237.

[20] P.N. Papanikolaou, J.N.E. Papaspyros, E.G. Kastrinakis, S.G. Nychas, A fast digital technique for calibration of hot-wires over a wide temperature range, Meas. Sci. Technol. 8 (1997) 1363–1366.

[21] J.M. Wallace, H. Eckelmann, R.S. Brodkey, The wall region in turbulent shear flow, J. Fluid Mech. 54 (1972) 39–48.

[22] S.G. Nychas, G.A. Sideridis, E.G. Kastrinakis, Momentum and heat transport in a quasi 2D flow. Turbulent wake of a cylinder interacting with a turbulent boundary layer, in: S. Gavrilakis, L. Machiels, P.A. Monkewitz (Eds.), Proceedings of the 6th European Turbulence Conference, Advances in Turbulence VI, Kluwer Academic Publishers, 1996, pp. 153–154.